



HHS Public Access

Author manuscript

Anal Chem. Author manuscript; available in PMC 2018 July 18.

Published in final edited form as:

Anal Chem. 2017 July 18; 89(14): 7758–7764. doi:10.1021/acs.analchem.7b01763.

Detection and Quantification of Hydrogen Peroxide in Aqueous Solutions Using Chemical Exchange Saturation Transfer

David Ryoo^{†,‡,§}, Xiang Xu^{†,‡}, Yuguo Li^{†,‡}, Joel A. Tang^{||}, Jia Zhang^{†,‡}, Peter C. M. van Zijl^{†,‡}, and Guanshu Liu^{†,‡,*}

[†]F. M. Kirby Research Center for Functional Brain Imaging, Kennedy Krieger Institute, Baltimore, Maryland [‡]Department of Radiology, Johns Hopkins University, Baltimore, Maryland 21205, United States [§]Department of Chemical & Biomolecular Engineering, Johns Hopkins University, Baltimore, Maryland 21205, United States ^{||}Department of Chemistry, Johns Hopkins University, Baltimore, Maryland 21205, United States

Abstract

The development of new analytical methods to accurately quantify hydrogen peroxide is of great interest. In the current study, we developed a new magnetic resonance (MR) method for noninvasively quantifying hydrogen peroxide (H₂O₂) in aqueous solutions based on chemical exchange saturation transfer (CEST), an emerging MRI contrast mechanism. Our method can detect H₂O₂ by its specific CEST signal at ~6.2 ppm downfield from water resonance, with more than 1000 times signal amplification compared to the direct NMR detection. To improve the accuracy of quantification, we comprehensively investigated the effects of sample properties on CEST detection, including pH, temperature, and relaxation times. To accelerate the NMR measurement, we implemented an ultrafast *Z*-spectroscopic (UFZ) CEST method to boost the acquisition speed to 2 s per CEST spectrum. To accurately quantify H₂O₂ in unknown samples, we also implemented a standard addition method, which eliminated the need for predetermined calibration curves. Our results clearly demonstrate that the presented CEST-based technique is a simple, noninvasive, quick, and accurate method for quantifying H₂O₂ in aqueous solutions.

Graphical Abstract

*Corresponding Author: guanshu@mri.jhu.edu.

ORCID

Guanshu Liu: 0000-0002-8188-4332

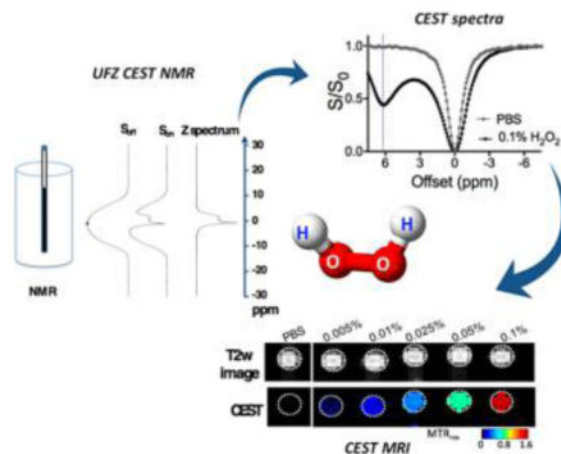
Notes

The authors declare no competing financial interest.

ASSOCIATED CONTENT

Supporting Information

The Supporting Information is available free of charge on the ACS Publications website at DOI: 10.1021/acs.anal-chem.7b01763. Effect of H₂O₂, saturation time and power and pH dependence impacts, H₂O₂ exchange rate estimation, and CEST MR repeatability and detectability (PDF)



Hydrogen peroxide (H_2O_2) is widely used in a variety of industrial applications.¹ It is the most versatile agent for pulp- and paper-bleaching,² treating pollutants, and eliminating organic and inorganic contaminants in wastewater.³ It is also an important biological molecule involved in redox processes, for instance as a key component in cell signaling pathways, and highly relevant to oxidative stress and inflammation.^{4,5} In tissue engineering, H_2O_2 is utilized as a highly efficient and clean oxygen generating agent that has been demonstrated to supply oxygen to transplanted stem cells.^{6,7} In the latter application, H_2O_2 -encapsulated polymeric carriers are incorporated into stem cell supporting scaffolds that contain catalase, and after being released from the carriers, H_2O_2 is hydrolyzed by catalase into H_2O and O_2 .^{8–11} Due to the importance of H_2O_2 , numerous analytical methods have been developed to detect and quantify it, including potassium permanganate titration,¹² infrared, Raman spectrophotometry,^{13,14} and fluorescence spectroscopy.¹⁵ Most of these methods however are destructive as they require the addition of reagents to the original samples. As a versatile noninvasive analytical tool, ^1H NMR spectroscopy has also been exploited for the quantification of H_2O_2 .^{16–19} For example, Stephenson and Bell quantified H_2O_2 using its unique ^1H NMR signal at around 10–11 ppm in both aqueous and nonaqueous solutions.¹⁷ Relaxometric NMR analysis can also report the detection of H_2O_2 due to its transverse relaxation time (T_2) enhancing ability.¹⁸ Unlike the method reported by Stephenson, NMR relaxometry has been applied to monitor heterogeneous catalysis systems dynamically, despite its detectability being only around 0.1%. Recently, another ultrasensitive ^1H NMR method was reported with a 20 μM detection limit.¹⁹ However, this method requires the combined use of $\text{DMSO-}d_6$, cryoprotective and low-temperature measurements (260 K or -13 °C) which required a total acquisition time of approximately 10 min.

In this study, we aimed to develop a new H_2O_2 detecting MR method using chemical exchange saturation transfer (CEST), a recently emerged MR contrast-generating technology.^{20–23} The CEST technology has been demonstrated in many studies for specifically detecting a wide array of labile protons of the exchange rate (k_{ex}) in the slow to intermediate regime (*i.e.*, $k_{\text{ex}} < \omega$, where ω is the chemical shift difference between the proton and water).^{24–26} The CEST principle can be applied to the detection of H_2O_2

because, in aqueous solution, H_2O_2 forms a hydrogen bonding network,²⁷ where each H in H_2O_2 interacts with two O atoms from neighboring H_2O_2 and OH^- , resulting in exchangeable protons with a chemical shift at ~ 11 ppm, or $\omega \sim 6.3$ ppm, making it quite suitable for CEST detection.²⁸ It should be noted that, different from NMR convention, the chemical shift offset by CEST MRI convention is defined as the frequency difference (ω) between a proton pool and water protons, which will be used in the rest of this work. In the present study, we sought to exploit this unique CEST signal for the accurate quantification of H_2O_2 in aqueous solutions. The acquisition speed of spectral detection can be significantly improved using a fast detection strategy, namely, ultrafast Z -spectroscopy (UFZ),^{29–31} making the method ideal for the quantification of uniform aqueous samples in a small volume. Moreover, as demonstrated in our studies, this method can be directly used for MRI detection of H_2O_2 without the need for any extra imaging agents.

MATERIALS AND METHODS

Chemicals and Sample Preparation

All compounds were purchased from Sigma (St. Louis, MO, USA). The concentration of H_2O_2 in the stock solution was verified using a Fluorimetric Hydrogen Peroxide Assay kit (Sigma). All the samples were prepared freshly immediately before NMR or MRI measurements.

Preparation of Samples for MR Imaging

All MRI samples were prepared using 1.5 mL Eppendorf tubes and transferred to 1 mm o.d. capillaries for MRI measurement.³² H_2O_2 solutions at concentrations of 0%, 0.005%, 0.01%, 0.025%, 0.05%, and 0.1%, corresponding to 0, 1.47, 2.94, 7.4, 14.7, and 29.4 mM, were prepared in 10 mM phosphate buffered saline (PBS) and titrated to pH = 6.0. To investigate the influence of sample relaxation times on CEST quantification, solutions of 0.05% H_2O_2 (7.4 mM, pH = 6.0) with different T_1/T_2 times were prepared by adding Gd-DTPA at final concentrations of 0.01, 0.1, and 0.5 mM.

MRI Measurement and Analysis

All *in vitro* MRI data sets were acquired at 37 °C on a 9.4 T Bruker Avance system equipped with a 20 mm birdcage RF coil using a previously reported protocol.³² A modified single slice rapid acquisition with relaxation enhancement (RARE) pulse sequence was used to acquire CEST weighted images with saturation offset frequencies from -8 to 8 ppm (step = 0.2 ppm) with respect to water resonance (set to 0 ppm by MRI convention). The imaging parameters were $T_R = 10$ s, effective $T_E = 43.2$ ms, RARE factor = 32, slice thickness = 1 mm, matrix size = 64×64 , resolution = 0.25×0.25 mm², and number of averages = 2. The saturation parameters were as follows: rectangular RF pulse; saturation times (T_{sat}) = 1, 2, 3, 4, and 6 s; and saturation field strengths (B_1) = 1.2, 2.4, 3.6, 4.7, and 5.9 μT . The WASSR method^{32,33} was used to correct B_0 inhomogeneity.

All data were processed using custom-written Matlab scripts. Conventionally, MTR_{asym} is used to quantify CEST effect by, to a large extent, removing other effects from the acquired Z -spectrum, including the water direct saturation effect and possible magnetization transfer

(MT) effects, which are assumed to be symmetric with respect to the water resonance.²³ The MTR_{asym} is defined as

$$MTR_{\text{asym}} = (S_{-\Delta\omega} - S_{+\Delta\omega}) / S_0 \quad (1)$$

where ω is the frequency difference of the protons of interest with respect to the water protons and S and S_0 are the signals acquired with and without saturation, respectively.

To achieve a linear relationship over a broad concentration range, we also adapted the MTR_{rex} metric³⁴ in our study, which is the reciprocal format of Z -spectral data:

$$MTR_{\text{rex}} = S_0 / S_{+\Delta\omega} - S_0 / S_{-\Delta\omega} \quad (2)$$

To achieve T_1 relaxation time compensated CEST quantification, we used the apparent exchange-dependent relaxation (AREX) metric:³⁴

$$\text{AREX} = MTR_{\text{rex}} / T_1 \quad (3)$$

Longitudinal (T_1) relaxation times of the samples were measured using a RARE-based saturation recovery sequence with eight T_R times ranging between 200 and 15,000 ms. T_1 values were estimated by fitting the ROI intensities to eq 4 using Matlab,

$$S(T_R) = S_0 \left[1 - \exp\left(-\frac{T_R}{T_1}\right) \right] \quad (4)$$

where $S(T_R)$ is the MRI signal at a certain T_R time, and the theoretical maximal MRI signal S_0 and T_1 time are the parameters to be estimated.

In addition, transverse (T_2) relaxation times were measured using the same RARE sequence with a CPMG preparation period inserted before the imaging readout.³⁵ The inter-echo time delay (τ_{CPMG}) was fixed at 10 ms, and the pulse numbers were varied from 4 to 1024. The acquisition time for each T_2 -weighted image was 25 s. T_2 relaxation times were estimated by fitting the ROI values to eq 5 using Matlab,

$$S(T_E) = S_0 \exp\left(-\frac{T_E}{T_2}\right) \quad (5)$$

where $S(T_E)$ are the MRI signal at each T_E time, and the theoretical maximal MRI signal S_0 and T_2 time are the parameters to be estimated.

Preparation of Samples for NMR Measurement

All NMR samples were prepared in 5 mm NMR tubes. To study the pH effect on CEST, the pH of H₂O₂ solutions (concentration = 0.025% or 7.4 mM) was titrated to 4, 4.5, 5.5, 6, 6.5, 7, 7.5, and 8. Concentration calibration curves at each pH were acquired using concentrations of 0, 0.0025%, 0.005%, 0.01%, 0.025%, and 0.05%, corresponding to 0, 0.74, 1.47, 2.94, 7.4, and 14.7 mM.

NMR Spectroscopy

All NMR measurements were acquired using a Bruker Avance 300 MHz spectrometer with a standard z gradient for dephasing. Nondeuterated samples were used for the study, and chemical shift referencing was with respect to the H₂O signal in the ¹H NMR spectrum. The gradient echo UFZ sequence shown in Figure 1a was utilized and saturation was achieved with a continuous wave RF power (B_1) of 5.7 μ T for duration (T_{sat}) of 1.6 s. A gradient field of 12.5 μ T/mm was applied concurrently with the RF saturation pulse along the Z -direction. To reduce the effect of eddy currents, a 5 ms delay was introduced between the saturation pulse gradient and the readout excitation pulse (4.29 μ s, 58.28 kHz). The dephasing/rephasing gradients were both 12.5 μ T/mm with opposite phases. As illustrated in Figure 1b, a reference scan (S_0) in which the saturation power was set at 0 was performed for signal normalization, *i.e.*, $S_{\text{norm}}(z) = S_{\text{on}}(z)/S_0(z)$. The normalization by S_0 can effectively cancel out the effect of B_0 inhomogeneity from the final Z -spectra. For each CEST experiment, the scan time was 1.7 s; however, a 20 s wait period was introduced between the reference and the CEST scan to allow the magnetization to fully recover. When not otherwise noted, all NMR measurements were conducted at 37 °C. The temperature effect of CEST quantification was studied by measuring the CEST signal of 0.1% H₂O₂ solutions (6.0 and 7.0) at 22, 27, 32, 37, 42, and 47 °C.

A standard addition (spiking) method was used to determine the H₂O₂ concentration in an unknown sample without predetermined calibration curves.³⁶ In brief, three groups of H₂O₂ solutions (pH 6.0) at concentrations of 0.01, 0.025, and 0.05% were used as “unknown” samples. In each group, four different T_1 times were achieved by adding Gd-DTPA at final concentrations of 0.01, 0.1, and 0.5 mM, resulting in a total of 12 unknown samples. After the first NMR measurement of each original sample, a 25 μ L standard H₂O₂ solution (concentration = 0.2% and pH = 6.0) was added to the NMR tube and CEST was measured again. The addition of spiking standard and CEST measurement were repeated three times. Assuming that the addition of small volumes of spiking standards did not change the properties of the original samples significantly, the measured CEST signal changes proportionally to the H₂O₂ concentration according to eq 6. Thus, a linear regression was performed on the plots of the measured CEST signal with respect to the concentration added at each time, and the original H₂O₂ concentration was estimated by the x -intercept of the extrapolated regression line,

$$\text{CEST}(V_{\text{add}}) = C \left(C_{\text{unknown}} \frac{V_0}{V_0 + V_{\text{add}}} + C_{\text{std}} \frac{V_{\text{add}}}{V_0 + V_{\text{add}}} \right) \quad (6)$$

where C is a constant, determined by the saturation parameters and the CEST properties of the exchangeable protons. V_0 and V_{add} are the volumes of the original sample and standard solution, respectively. C_{unknown} and C_{std} are the concentration to be determined and that of spiking standard solutions, respectively.

RESULTS AND DISCUSSION

CEST NMR and MRI Detection of H₂O₂ in Aqueous Solution

Unless otherwise noted, chemical shifts by the magnetization transfer MRI convention are used throughout this work. Whereas only a small T_2 contrast and negligible T_1 contrast can be detected (Figure S1, Supporting Information), H₂O₂ (0.1%, pH 6.0, and 37 °C) produced a distinct CEST signal at 6.2 ppm (Figure 2a,b). The 6.2 ppm CEST signal is attributed to the H atoms in the H₂O₂-H₂O hydrogen bond network. This chemical shift is slightly smaller than the 6.3 ppm reported by Stephenson and Bell (acquired at room temperature)¹⁷ possibly due to the fact that our studies were carried out at 37 °C. The 1.5 ppm signal is attributed to the H₂O (or OH⁻) interacting with H₂O₂, which is consistent with the NMR spectroscopic study of H₂O₂ in aqueous solution.³⁷ Alternatively, this could be a broader component toward the water frequency which may be due to partial coalescence with water protons. Figure 2b shows that 0.1% H₂O₂ (~30 mM per molecule or 60 mM per exchangeable proton) produced a remarkable CEST effect, *i.e.*, an MTR_{asym} of 0.543, corresponding to a 54.3% change in water signal, using a saturation pulse of 4.7 μT and 4 s. Considering the concentration of water protons is 110 M, our result suggests that CEST detection achieved an amplification ratio of $(54.3\% \times 110 \text{ M}) / (60 \text{ mM}) \approx 1000$. It should be noted that the CEST signal highly depends on saturation parameters such as B_1 and T_{sat} (Figure S2, Supporting Information). The exchange rate of H₂O₂ was estimated to be 460 and 1.4 kHz for CEST signals at 1.5 and 6.2 ppm, respectively, at pH 6.0 and 37 °C using the Bloch fitting of QUEST data (Figure S3, Supporting Information),³⁸ in good agreement with previous reports.²⁸ This specific CEST signal hence allows a high spatial resolution MRI detection of H₂O₂ as shown in Figure 2c. Our results show that CEST MRI can be used to detect H₂O₂ in solution down to the millimolar concentration range (0.005% = 1.47 mM). Figure 2d showed that concentration dependence of two CEST quantification metrics, MTR_{asym} and MTR_{rex}, with the former fitted with a linear function and the later fitted with the Michaelis–Menten function.³⁹ Among them, the MTR_{rex} provides a larger dynamic range linearly with the concentrations of H₂O₂ and therefore was chosen to quantify the CEST signal of H₂O₂ in the rest of this work.

CEST Quantification as a Function of T₁ Times

To investigate the confounding effects of sample T_1 relaxation times on CEST quantification, we prepared 0.1% H₂O₂ solutions doped with different Gd-DTPA and acquired the CEST signal of them. As shown in Figure 3a, after the addition of Gd-DTPA, sample T_1 relaxation times decreased from 3.670 ± 0.017 to 0.591 ± 0.005 s, and in Figure 3b, T_2 times decreased from 2.618 ± 0.072 s to 0.403 ± 0.005 s. As expected, the decrease in T_1 times resulted in a striking reduction in CEST signal (Figure 3c). For example, when T_1 was changed from 3.67 to 0.59 s, MTR_{asym} decreased by 72% (Figure 3d) and MTR_{rex} by 78% (Figure 3e), the same within error as expected for an inverse parameter. In contrast,

when the apparent exchange-dependent relaxation (AREX) parameter, a previously reported relaxation time compensated CEST metric,³⁴ was used, the relative change was reduced to 0.5% (AREX = 0.103 ± 0.003) and 6.9% (AREX = 0.110 ± 0.003) for samples with 0.01 mM ($T_1 = 3.32$ s) and 0.1 mM ($T_1 = 1.70$ s) Gd-DTPA, respectively, compared to the sample without Gd-DTPA (AREX = 0.103 ± 0.004 and $T_1 = 3.67$ s). Even when 0.5 mM Gd-DTPA was added ($T_1 = 0.59$ s), the AREX was calculated to be 0.127 ± 0.004 , corresponding to a relatively small change of 22.9%. The relatively large error may be caused by markedly shortened T_2 time by Gd-DTPA (*i.e.*, changed from 2.62 to 0.4 s). Our results suggested that using AREX to quantify the CEST signal of H₂O₂ could effectively compensate the confounding effect of relaxation times up to a certain limit and improve the CEST quantification when the changes in T_1 relaxation times are not dramatic.

pH Dependence of the CEST Signal of H₂O₂

Since proton exchange is either acid- or base-catalyzed, the solution pH often affects the CEST signal strongly. The pH effect on the CEST signal of H₂O₂ is clear from the changes in the Z -spectral shape of H₂O₂ solutions at different pHs (Figure 4a). To fully investigate the pH dependence, we measured the CEST signal of 0.025% H₂O₂ from pH 2 to pH 8 at 6.2 ppm (Figure 4b). In the pH range studied, 0.025% H₂O₂ produced the strongest CEST signal at pH ~ 6, *i.e.*, an MTR_{rex} of 0.182 ± 0.015 . In the pH range from 5 to 8, where base catalysis is the dominant mechanism,²⁷ exchange rates increase with increasing pH. Hence, the CEST signal increased with increasing pH in the pH range of 5–6. However, when pH was higher than 6.0, because the exchange rate becomes too fast, the CEST signal decreased with increasing pH. For example, the MTR_{rex} at pH 7.5 is only 0.062 ± 0.006 , approximately 34.1% of that at pH 6.0. When pH is below 5.0, the proton exchange is dominated by acid-catalysis mechanism and exchange rates increase with decreasing pH.²⁷ Similar to the trend showing in the pH range of 5–8, the CEST signal first slightly increases when pH drops from 5 to 4 and then decreases steeply when pH further decreases from 4 to 2 because exchange rates become too fast.

Temperature Dependence of the CEST Signal H₂O₂

Similar to pH, temperature may strongly affect proton exchange rates and hence CEST signals. As such, we investigated the effect of temperature on the CEST signal of H₂O₂ over the range from 22 to 47 °C. As shown in Figure 4c, a strong negative temperature dependence can be observed on the CEST signal of H₂O₂ solutions (0.1%) at pH 6.0 and 7.0. For example, when temperature increased from 22 to 37 °C, the MTR_{rex} of 0.1% H₂O₂ at pH 6.0 dropped by 34% (from 0.922 to 0.608) and that at pH 7.0 dropped by 55% (from 0.329 to 0.148). This negative temperature dependence at these pH values can be attributed to the increased exchange rates at higher temperature following the Arrhenius equation.^{28,40} Because the exchange rate of H₂O₂ is already in the intermediate regime when pH > 6, an increased exchange rate would reduce the apparent CEST signal due to coalescence of the H₂O₂ proton resonance with the water proton resonance. Our results therefore suggest that measuring at a low temperature may potentially improve the sensitivity of CEST detection greatly when pH > 6. Moreover, the temperature should be assured to be constant throughout the CEST measurement series.

CEST Detectability

To determine the CEST MR detectability at each pH, defined as the minimal concentration that CEST MR can reliably detect for the current RF coil, we first acquired the calibration curves of H₂O₂ at different pH values over the concentration range from 0.74 to 14.7 mM. To avoid systematic errors, three independent measurements were performed on different days with samples freshly prepared each time. As shown in Figure 5, the obtained calibration curves showed a good linearity for all pHs. Then we used the Student's *t* test (two-tailed and paired) to determine the minimal concentration generating a statistically significant CEST signal (*i.e.*, $P > 0.005$) with respect to that of simple PBS samples, and listed the results in Table S-1 (Supporting Information). At most pH values, CEST detectability was about 1.5 mM; the highest detectability (~0.74 mM) could be achieved at pH 5.5 and pH 6.0, whereas the lowest detectability (~14.7 mM) was observed at pH 8.0. Our results imply that a millimolar level detectability can be achieved except for H₂O₂ in solutions with basic pH, providing a more sensitive and fast approach than traditional NMR methods. For comparison, the fast relaxometry-based NMR approach was reported to have a detectability ~ 0.1% (29.4 mM) for pH between 4.5 and 5.5, and 0.5% (147 mM) when pH = 7.¹⁸ Our method appears to be 2 orders of magnitude more sensitive. The ¹H NMR technique reported by Stephenson and Bell had a detection limit down to 1 mM in aqueous solution at 21 °C using a 400 MHz NMR spectrometer, with a temporal resolution of 30 s,¹⁷ with a line width, however, of over 250 Hz. Considering our CEST NMR measurements were conducted at 37 °C using a lower field scanner (300 MHz) and at an acquisition time of ~2 s, our method is indeed more sensitive and, more importantly, readily applied to inhomogeneous samples.²⁹ However, it should be noted that the actual detectability also depends on the level of noise, which can be strongly affected by the hardware and experiment condition in an MRI or NMR study.

Another ¹H NMR method was recently reported by Constantinos et al. to have a detection limit of 20 μM.¹⁹ However, it required the combination of DMSO-*d*₆, cryoprotection, a low measurement temperature (-13 °C), and a long acquisition time (10 min). In contrast, our approach does not require specific agents and sample preparation procedure, and measurement conducted at 37 °C, hence, could have a broader application. Moreover, based on the temperature dependence studies shown in Figure 4d, our CEST MRI can also gain much higher sensitivity at a low temperature.

Quantification of H₂O₂ Using Standard Addition

While calibration curves such as those shown in Figure 5 can be used to quantify H₂O₂ in unknown samples, an accurate CEST quantification requires measurements of pH and *T*₁ relaxation times, and use of acquisition parameters identical to those used for the predetermined calibration curves. It is highly desirable to have a more robust method that can be used to quantify H₂O₂ without the need for *a priori* calibration curve. To this end, we used a standard addition (spiking) strategy, a commonly used analytical technique to overcome matrix interference.³⁶ To demonstrate the utility of this standard addition method, we chose to vary the sample *T*₁ time among the three most confounding factors (pH, temperature, and *T*₁ time) and set it as the unknown factor in the present study. Sample *T*₁ times were adjusted from 3.2 to 0.6 s using Gd-DTPA. CEST signals before and after each

addition of standard solution were measured and plotted as the final concentrations of standard solution added (eq 6).

Figure 6a shows that the original concentration of H_2O_2 in the sample can be determined by the x -intercept of the linear regression. Our results showed that the linear regression with three additions fitted well with the experimental data and, except in the sample with dramatically shortened T_1 , provided an excellent estimation of the original concentration, *i.e.*, measured concentration (C_{measured}) = $0.010 \pm 0.001\%$ for all the samples (true concentration $C_{\text{true}} = 0.01\%$). When T_1 was 0.6 s, C_{measured} was estimated to be $0.015 \pm 0.003\%$. To investigate how many additions are required to generate an accurate estimation, we compared the measured H_2O_2 concentration as a function of the number of standard additions. As shown in Figure 6b, except the samples with very short T_1 , the results obtained using one addition produced a 30–40% error ($C_{\text{measured}} = 0.013\text{--}0.014\%$) and those for the two addition protocol a 10–20% error ($C_{\text{measured}} = 0.011\text{--}0.012\%$), indicating that a three addition should be used to obtain sufficiently high accuracy.

Using the same three standard addition method, we also measured H_2O_2 samples with concentrations of 0.025 and 0.05%, and correlated the measured H_2O_2 concentrations with their true values. Both the correlation study (Figure 6c) and Bland–Altman analysis (Figure 6d) showed a very good agreement between C_{measured} and C_{true} in each T_1 time group; *i.e.*, the Pearson correlation coefficients (R_2) were 0.9994, 0.9998, 0.9998, and 0.9750 and the slopes of fitted lines were 1.167 ± 0.1324 , 1.002 ± 0.00989 , 1.005 ± 0.00584 , and 0.9928 ± 0.009549 for T_1 of 0.6, 1.7, 2.9, and 3.2 s, respectively. For T_1 times of 3.2, 2.9, 1.7, and 0.6 s, respectively. The data point for 0.05% H_2O_2 at T_1 time of 0.6 s is considered an outlier and excluded from the fitting. This outlier may be caused by the small signal increase after each addition when the concentration of the original solution is close to the standard solution (0.05% vs 0.2%) and only a small volume was added each time (*i.e.*, 25 μL each time to an original 475 μL volume). To obtain high accuracy, one should always use the standard solution at a sufficiently high concentration. In addition, using high concentration standard solutions allows the use of smaller addition volumes, which can effectively reduce the potential impact of the addition solutions on the original solution properties, such as T_1 times and pH.

Nevertheless, our results clearly demonstrated that accurate measurement of H_2O_2 concentration could be achieved using the standard addition approach, eliminating the need for a predetermined calibration curve, which best fits the measurement of a few samples. For high-throughput screening of a large volume of samples, the standard addition may result in a significant increase of measurement time. The standard addition is also not suitable for monitoring the change in H_2O_2 dynamically. In these scenarios, the standard method with predetermined calibration curves still should be used.

CONCLUSIONS

In the present study, we successfully developed a new MR method for the quantification of H_2O_2 in aqueous solutions using the CEST principle. The potential effects of sample properties, including pH, temperature, and relaxation times, on CEST MRI detection were

comprehensively investigated. We used a recently developed UFZ CEST method to greatly boost the acquisition speed to be on the order of seconds. Furthermore, we demonstrated the use of the standard addition method to accurately determine the H₂O₂ concentration in unknown samples without the need for predetermined calibration curves. Our results clearly show that the present CEST-based technique is a noninvasive, quick, and accurate quantitative method for detecting H₂O₂ in aqueous solutions.

Compared to other available analytical methods, the proposed CEST method has a number of tempting advantages. First, the CEST mechanism provides a great amplification of the NMR signal of exchangeable protons. For instance, our results show that 0.1% H₂O₂ (~60 mM exchange proton) can generate a CEST effect of 54.3% (MTR_{asym}), corresponding to an amplification ratio of ~1000. Second, the CEST NMR method is a noninvasive and simple method that can directly detect H₂O₂ in aqueous solution without the need for sample extraction and the use of deuterated solvents. Third, the UFZ CEST method allows ultrafast acquisition, *e.g.*, <2 s per Z-spectrum in the current study, which no doubt is highly desirable for many applications where the H₂O₂ concentration needs to be monitored dynamically with high temporal resolution. Furthermore, the ease of sample preparation and fast acquisition allows the utilization of the standard addition approach to quantify H₂O₂ without the need for *a priori* information on the sample properties nor a predetermined calibration curve. Finally, as demonstrated in our study, CEST also allows MRI detection, which can be further accelerated by incorporating the UFZ approach, making this method potentially useful for heterogeneous samples and biomedical imaging, implying the proposed method has a broad spectrum of potential applications.

Supplementary Material

Refer to Web version on PubMed Central for supplementary material.

Acknowledgments

This work was supported by National Institutes of Health (NIH) Grants R03EB021573, R01CA211087, R21CA215860, and R01EB015032.

References

1. Jones, CW. Applications of hydrogen peroxide and derivatives. Vol. 2. Royal Society of Chemistry; 1999.
2. Hage R, Lienke A. *Angew Chem, Int Ed.* 2005; 45:206–222.
3. Pardieck DL, Bouwer EJ, Stone AT. *J Contam Hydrol.* 1992; 9:221–242.
4. Rhee SG. *Science.* 2006; 312:1882–1883. [PubMed: 16809515]
5. Veal EA, Day AM, Morgan BA. *Mol Cell.* 2007; 26:1–14. [PubMed: 17434122]
6. Oh SH, Ward CL, Atala A, Yoo JJ, Harrison BS. *Biomaterials.* 2009; 30:757–762. [PubMed: 19019425]
7. Harrison BS, Eberli D, Lee SJ, Atala A, Yoo JJ. *Biomaterials.* 2007; 28:4628–4634. [PubMed: 17681597]
8. Ng SM, Choi JY, Han HS, Huh JS, Lim JO. *Int J Pharm.* 2010; 384:120–127. [PubMed: 19819316]
9. Abdi SI, Ng SM, Lim JO. *Int J Pharm.* 2011; 409:203–205. [PubMed: 21356297]
10. Abdi SI, Choi JY, Lau HC, Lim JO. *Tissue Eng Regen Med.* 2013; 10:131–138.
11. Bae SE, Son JS, Park K, Han DK. *J Controlled Release.* 2009; 133:37–43.

12. Huckaba CE, Keyes FG. *J Am Chem Soc.* 1948; 70:1640–1644. [PubMed: 18915785]
13. Vacque V. *Spectrochimica Acta Part A: Molecular Spectroscopy.* 1997; 53:55–66.
14. Vacque V, Dupuy N, Sombret B, Huvenne JP, Legrand P. *Appl Spectrosc.* 1997; 51:407–415.
15. Lazrus AL, Kok GL, Gitlin SN, Lind JA, McLaren SE. *Anal Chem.* 1985; 57:917–922.
16. Monakhova YB, Diehl BWK. *Anal Methods.* 2016; 8:4632–4639.
17. Stephenson NA, Bell AT. *Anal Bioanal Chem.* 2005; 381:1289–1293. [PubMed: 15756600]
18. Buljubasich L, Blumich B, Stapf S. *Chem Eng Sci.* 2010; 65:1394–1399.
19. Tsiafoulis CG, Gerotheranassis IP. *Anal Bioanal Chem.* 2014; 406:3371–3375. [PubMed: 24652156]
20. van Zijl PC, Yadav NN. *Magn Reson Med.* 2011; 65:927–948. [PubMed: 21337419]
21. Ward K, Aletras A, Balaban R. *J Magn Reson.* 2000; 143:79–87. [PubMed: 10698648]
22. van Zijl PCM, Sehgal AA. *eMagRes.* 2016; 5:1307–1332.
23. Liu G, Song X, Chan KW, McMahon MT. *NMR Biomed.* 2013; 26:810–828. [PubMed: 23303716]
24. Li Y, Chen H, Xu J, Yadav NN, Chan KW, Luo L, McMahon MT, Vogelstein B, van Zijl PC, Zhou S, Liu G. *Oncotarget.* 2016; 7:6369–6378. [PubMed: 26837220]
25. Liu G, Bettgowda C, Qiao Y, Staedtke V, Chan KW, Bai R, Li Y, Riggins GJ, Kinzler KW, Bulte JW, McMahon MT, Gilad AA, Vogelstein B, Zhou S, van Zijl PC. *Magn Reson Med.* 2013; 70:1690–1698. [PubMed: 24123389]
26. Liu H, Jablonska A, Li Y, Cao S, Liu D, Chen H, Van Zijl PC, Bulte JW, Janowski M, Walczak P, Liu G. *Theranostics.* 2016; 6:1588–1600. [PubMed: 27446492]
27. Anbar M, Loewenstein A, Meiboom S. *J Am Chem Soc.* 1958; 80:2630–2634.
28. Zhang, S. Direct Detection of Hydrogen Peroxide via ¹H CEST-MRI. Proceedings of the Joint Annual Meeting ISMRM-ESMRMB; May 19–25, 2007; Berlin, Germany. Concord, CA, USA: International Society for Magnetic Resonance in Medicine; 2007.
29. Xu X, Lee JS, Jerschow A. *Angew Chem, Int Ed.* 2013; 52:8281–8284.
30. Boutin C, Leonce E, Brotin T, Jerschow A, Berthault P. *J Phys Chem Lett.* 2013; 4:4172–4176. [PubMed: 24563724]
31. Xu X, Yadav NN, Song X, McMahon MT, Jerschow A, van Zijl PC, Xu J. *J Magn Reson.* 2016; 265:224–229. [PubMed: 26969814]
32. Liu G, Gilad AA, Bulte JW, van Zijl PC, McMahon MT. *Contrast Media Mol Imaging.* 2010; 5:162–170. [PubMed: 20586030]
33. Kim M, Gillen J, Landman B, Zhou J, van Zijl P. *Magn Reson Med.* 2009; 61:1441–1450. [PubMed: 19358232]
34. Zaiss M, Xu J, Goerke S, Khan IS, Singer RJ, Gore JC, Gochberg DF, Bachert P. *NMR Biomed.* 2014; 27:240–252. [PubMed: 24395553]
35. Yadav NN, Xu J, Bar-Shir A, Qin Q, Chan KW, Grgac K, Li W, McMahon MT, van Zijl PC. *Magn Reson Med.* 2014; 72:823–828. [PubMed: 24975029]
36. Ellison SL, Thompson M. *Analyst.* 2008; 133:992–997. [PubMed: 18645637]
37. Gun'ko V, Turov V, Turov A. *Chem Phys Lett.* 2012; 531:132–137.
38. McMahon MT, Gilad AA, Zhou J, Sun PZ, Bulte JWM, van Zijl PCM. *Magn Reson Med.* 2006; 55:836–847. [PubMed: 16506187]
39. Ali MM, Liu G, Shah T, Flask CA, Pagel MD. *Acc Chem Res.* 2009; 42:915–924. [PubMed: 19514717]
40. Zhang S, Malloy CR, Sherry AD. *J Am Chem Soc.* 2005; 127:17572. [PubMed: 16351064]

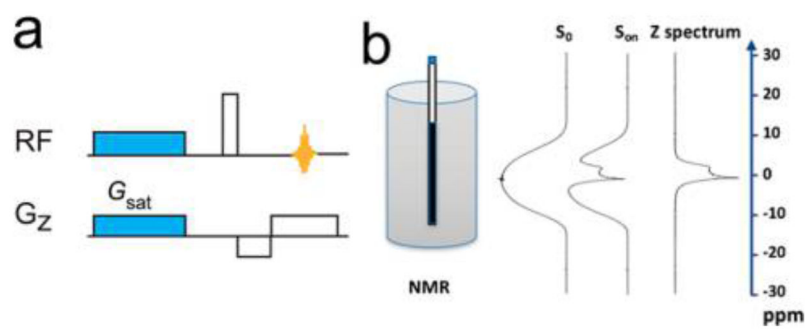


Figure 1. Illustration of (a) UFZ pulse sequence and (b) how to generate a Z -spectrum using the UFZ method.

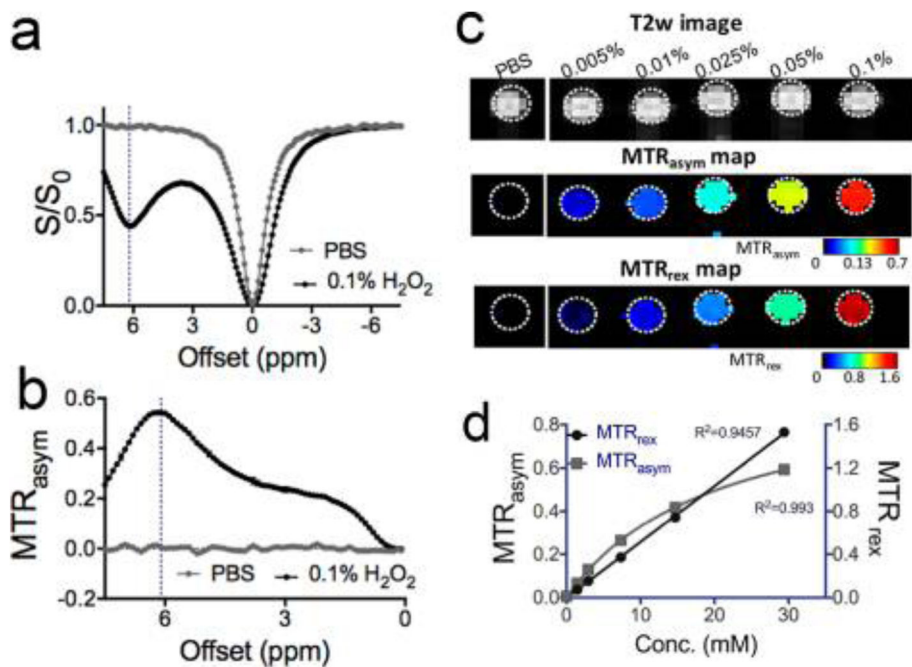


Figure 2. CEST MRI detection of H₂O₂: (a) Z-spectra and (b) MTR_{asym} plots of 0.1% H₂O₂ in pH 6.0 PBS and just PBS solution; (c) T₂-weighted image, MTR_{asym} map, and MTR_{rex} map of six samples containing different H₂O₂ in pH 6.0 PBS; (d) concentration dependence of the mean CEST signals (triplicate), as quantified by MTR_{asym} and MTR_{rex}.

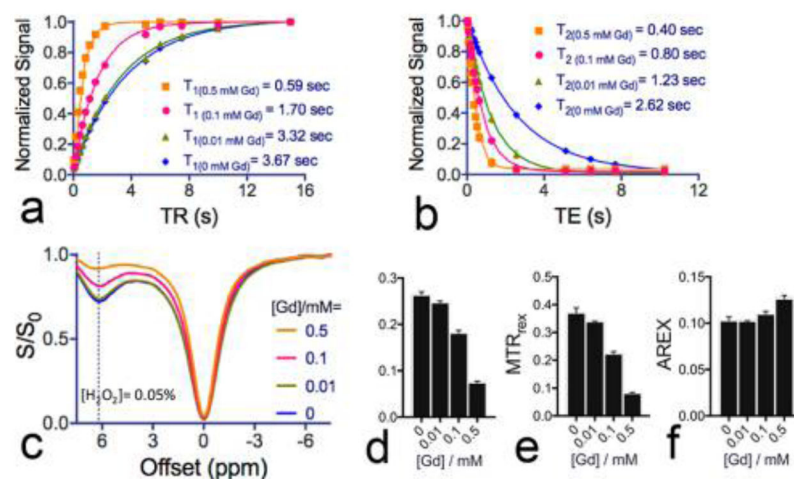


Figure 3. Quantification of the CEST signals of H_2O_2 samples with different T_1 and T_2 relaxation times: (a) T_1 and (b) T_2 measurements of four samples containing different concentrations of Gd-DTPA and 0.1% H_2O_2 ; (c) corresponding Z-spectra of the four samples; (d) MTR_{asym} , (e) MTR_{rex} , and (f) AREX of the four samples based on the Z-spectra shown in panel c.

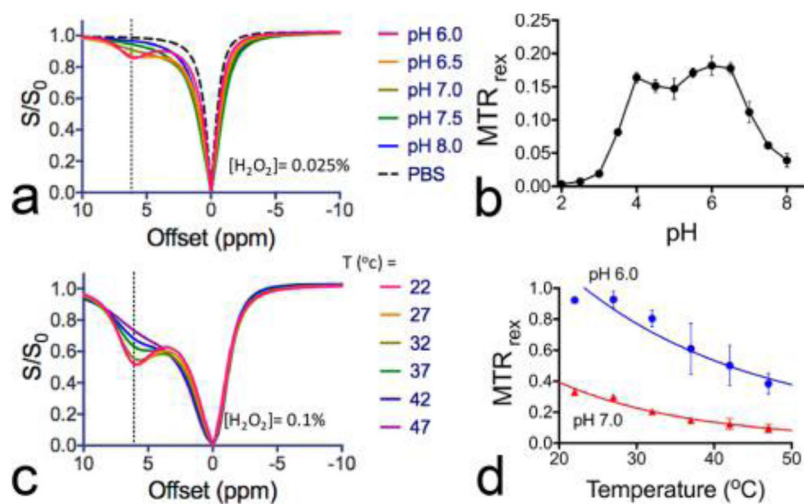


Figure 4. Effects of pH and temperature on the CEST signal of H₂O₂: (a) Z-spectra and (b) MTR_{rex} values at 6.2 ppm of H₂O₂ solution at different pHs at 37 °C; (c) Z-spectra and (d) MTR_{rex} values at 6.2 ppm of pH 6.0 and pH 7.0 H₂O₂ solutions at different temperatures (dots) and the fitting of the temperature data into the Arrhenius equation³⁹ (lines).

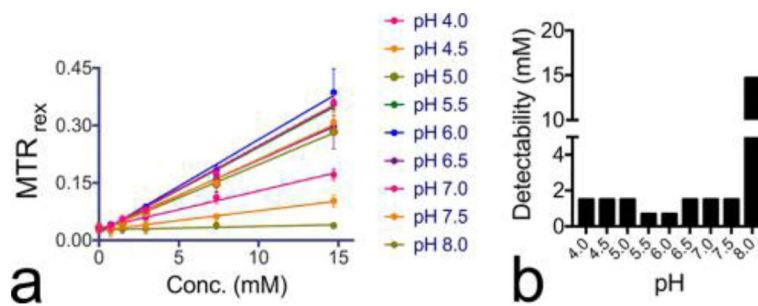


Figure 5. (a) Calibration curves of H_2O_2 solutions at different pHs; (b) detectability of H_2O_2 at different pHs.

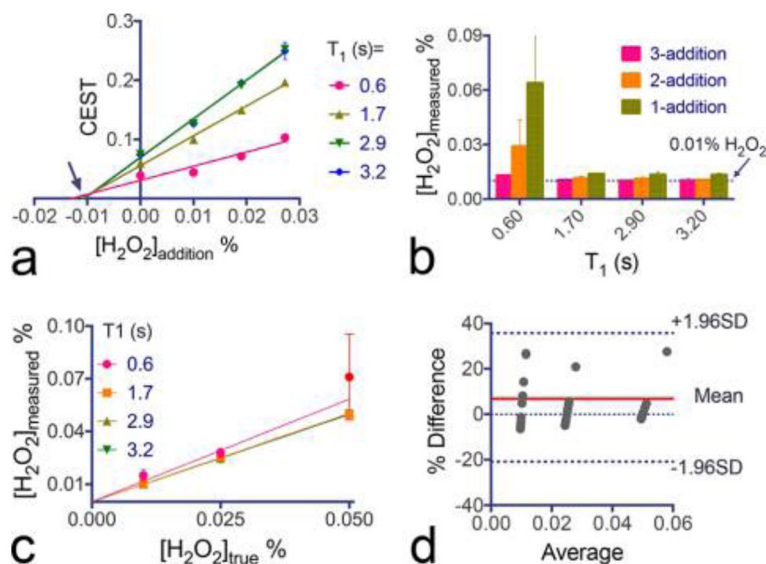


Figure 6. Linear regression of H₂O₂ and Gd-DTPA mixture using three additions of spiking standard solutions: (a) linear regression of the CEST signals before and after three additions of 0.2% H₂O₂ standard solution (25 μL each time to an original 475 μL volume; the arrow points to the true original H₂O₂ concentration (0.01%)); (b) measured H₂O₂ concentrations using different numbers of standard addition, from 1 to 3, for the same 0.01% H₂O₂ with T₁ times; (c) correlation and (d) Bland–Atman plot of the measured H₂O₂ concentrations and the “true” concentrations for all three H₂O₂ concentrations and four different T₁ times, where x-axis and y-axis are the average and difference (%) of the measured concentration and the “true” values, respectively. All data points are shown as mean ± standard deviations of triplicate samples.